Numerical simulation of heat transfer in the near-wall region of tubular reactors packed with metal open-cell foams

Enrico Bianchi [a], Gianpiero Groppi [b], Wilhelm Schwieger [a], Enrico Tronconi [b], Hannsjörg Freund [a,*]

[a] Lehrstuhl für Chemische Reaktionstechnik, Friedrich-Alexander-Universität Erlangen-Nürnberg, Egerlandstr. 3, Erlangen D-91058, Germany
[b] Laboratory of Catalysis and Catalytic Processes, Dipartimento di Energia, Politecnico di Milano, Piazza Leonardo da Vinci 32, Milano 20133, Italy

Received 30 July 2014
Received in revised form 3 November 2014
Accepted 8 November 2014
Available online 15 November 2014

1. Introduction

In non-adiabatic fixed bed reactors the use of structured catalyst supports offers superior control on the bed transport characteristics with the possibility to adjust the support properties in an optimal manner. In this regard, open-cell metallic foams (sometimes referred to as sponges) are characterized by particularly promising features. Their light structure, with a porosity generally higher than 80%, is less prone to excessive pressure drop [1–3] even in applications with high spatial velocities. At the same time, the relatively high value of the surface area density [4–6] allows for realizing reasonably high catalyst loads in the reactor [7,8]. Moreover, the continuity of the solid support provides an additional path for the heat flux, particularly in the case of foams made of highly conductive metals, without the problem of preventing radial mixing as encountered in monolithic honeycomb structures.

It is worth noticing that, despite a general similarity between the physical processes, a main difference exists in the relative importance of heat transfer mechanisms in open-cell foams on the one side and conventional packed beds on the other side. For example, in a particle random packing the near wall region is generally characterized by different hydrodynamic conditions, because the void fraction is not constant but much higher close to the reactor wall [9]. Moreover, the role of inter-particle conduction is extremely weak as a result of the finite number of confined point contacts. The conduction inside the interconnected solid matrix of consolidated porous media such as open-cell foams, in contrast, is quite significant and may even represent the main contribution to heat transfer for systems operating with low conductive fluids and/or low flow rates [6,10].

For these reasons, the correlations for the effective heat transfer coefficients that are available in literature [11] from extensive analysis of unconsolidated packed beds are not directly applicable to open-cell foam beds [12]. Instead, new data must be collected and evaluated for the specific application. Open-cell foams made

* Corresponding author.
E-mail address: hannsjoerg.freund@fau.de (H. Freund).

Nomenclature

List of symbols

A [m^2] area of the heated surface
Bi [–] Biot number
c [J kg^{-1} K^{-1}] specific heat capacity
D_h [m] hydraulic channel diameter
d_h [m] hydraulic pore diameter, $\frac{4\varepsilon}{S_v}$
d_p [m] average pore inner diameter
d_c [m] average cell inner diameter
e [J kg^{-1}] specific internal energy
F [–] Forchheimer inertial coefficient
H [m] height of the 3D foam model
Hg [–] Hagen number, $\frac{\Delta p}{\Delta L}\frac{\rho u d_h^3}{\mu^2}$;
h_i [W m^{-2} K^{-1}] interphase heat transfer coefficient
h_U [W m^{-2} K^{-1}] heat transfer coefficient between the fluid and the unfinned wall
h_W [W m^{-2} K^{-1}] wall heat transfer coefficient
k [W m^{-1} K^{-1}] thermal conductivity
k_f [W m^{-1} K^{-1}] fluid thermal conductivity
k_s [W m^{-1} K^{-1}] solid thermal conductivity
k_e [W m^{-1} K^{-1}] effective conductivity of the foam bed
K [m^2] permeability
L [m] length of the 3D foam model
m [m^{-1}] equivalent Biot number for a single strut;
M [m^{-1}] corrected m coefficient for open-cell foam structure;
Nu [–] Nusselt number at the wall, $\frac{h_w d_p}{k_f}$
p [Pa] pressure
Pe [–] Peclet number based on interstitial velocity, $\frac{\rho u c_f d_p}{\varepsilon k_f}$
Pr [–] Prandtl number, $\frac{\mu c_f}{k_f}$
q [W m^{-2}] heat flux for unit area
R [m K W^{-1}] thermal resistance
Re [–] Reynolds number based on pore diameter and interstitial velocity, $\frac{\rho u d_p}{\varepsilon\mu}$
S [m^2] interphase open-cell foam area
S_v [m^{-1}] geometric interfacial area density, or volumetric surface, of foam
t_s [m] average middle strut section
T [K] temperature
u [m s^{-1}] velocity
U [W m^{-2} K^{-1}] overall heat transfer coefficient
W [m] width of the 3D foam model
X, Y, Z [m] Cartesian coordinates

Greek symbols

Γ [m^2] channel cross sectional area
ε [–] bed porosity
η [–] efficiency
μ [kg s^{-1} m^{-1}] dynamic viscosity of fluid
ρ [kg m^{-3}] mass density
τ [Nm^{-2}] viscous stress tensor

Subscripts

b bulk
c cell
e effective
f fluid properties
F fin
h hydraulic
i interphase
in inlet
lm logarithmic mean
n normal
out outlet
p pore
q fixed heat flux
s solid properties
T fixed temperature
U unfinned
w wall
x, y, z Cartesian coordinates

of highly conductive metals were investigated in several studies [13–16] for pure air thermal exchanger, such as compact heat sinks. However, in none of these previous studies the effect of the coupling between the foam packing and the heated surface was considered, as the metal sample was directly brazed with the exchanger walls. Owing to the high solid matrix conductivity, such a configuration leads to a relatively homogeneous temperature distribution which can be described by a 1D model for the heat transport.

In contrast, if the open-cell foam is used as catalyst support it is packed inside the reactor and thus a gap will always exist between the foam and the externally cooled or heated reactor wall. For this case, a two dimensional description of the temperature profile with a 2 parameter model is more appropriate [17]. In previous experimental studies an annulus of small, but finite size was always present between the support and the reactor wall. In some cases it was attempted to minimize the gap influence by the use of layers of carbon foil to wrap the foam samples in order to avoid bypassing in the experimental set-up [18]. In any case it becomes obvious that the size of this gap and its influence on the flow and transport properties must be considered. However, only few data are available in literature to estimate the heat transfer coefficients in the near wall region of an open-cell foam bed.

Previous publications mainly report on experimental studies of heat transfer with air in the laminar flow regime, where, e.g., a correlation for the heat wall coefficient was derived for an individual Al_2O_3 foam [17]. In another study, the average value of this parameter was estimated for different β-SiC or polyurethane foams [19]. A few estimates of the wall heat transfer coefficient for an aluminium foam and two-phase flow are also available [20]. However, in neither of these studies the effect of the gap size is considered at all. In a recent study [21], based on metal foam samples with different gas flow rates, it was pointed out that the thermal continuity was not assured despite the tight fit between the samples and the reactor wall. Nevertheless, despite the gap existence was postulated, the effect of the gap itself was not focus in these previous investigations, mainly due to the difficulty and high uncertainty in measuring this parameter in the experimental set-up.

To overcome the limitations of experimental set-ups, in this work a numerical study is therefore proposed. In fact, computational fluid dynamics (CFD) represents an appropriate method to perform a detailed analysis and characterization of thermal and fluid phenomena within catalytic fixed bed reactors [22–24]. In addition, the use of such simulations as numerical experiments allows to fully control the operative condition and the gap size at the wall. Based on these simulations, the purpose of this study is

to systematically investigate the effect of different wall coupling scenarios on the thermal performance of the system. The final goal is to identify correlations for the effective heat transfer coefficients necessary for a simplified 2D description of a reactor packed with an open-cell metal foam.

To achieve this goal, the 3D models of two different open-cell foams, both made of aluminium, are used in this study. Moreover, air as well as water is considered as working fluid in the simulations. While the majority of experimental heat transfer data were collected in gas–solid set-ups [17,19,21], in many processes the operative fluid is liquid [25]. Thus, in the present work the simulated fluids are both air, for comparison and validation purposes, and water, to also explore liquid–solid systems. Another aspect to be considered is the flow regime. As observed in literature [26], the majority of experimental data lie in the laminar flow regime; however, many industrial processes are operated in the turbulent regime. For this reason, the flow rates explored in the present simulation studies cover a wide range in order to also include the turbulent flow regime. Summing up, the detailed CFD simulation studies performed in this work allow for the investigation of a number of well-defined system configurations including those that are not easily accessible by experimental approaches.

2. Numerical model and mesh generation

The investigation of the mechanisms responsible for the heat transfer between the reactor wall and the solid foam was performed in detail by finite volume analysis (FVA). The mesh generator and the solver for the FVA were implemented in the open source environment OpenFOAM v2.1.1 [27], a general library of C++ classes for numerical simulation [28] mainly used for computational fluid dynamics (CFD) simulations [29].

With the purpose to validate the results of the simulations with literature data, three different classes of studies were performed: estimation of pressure drop (without heat addiction through the boundaries), evaluation of the interphase heat transfer, and conjugated heat transfer.

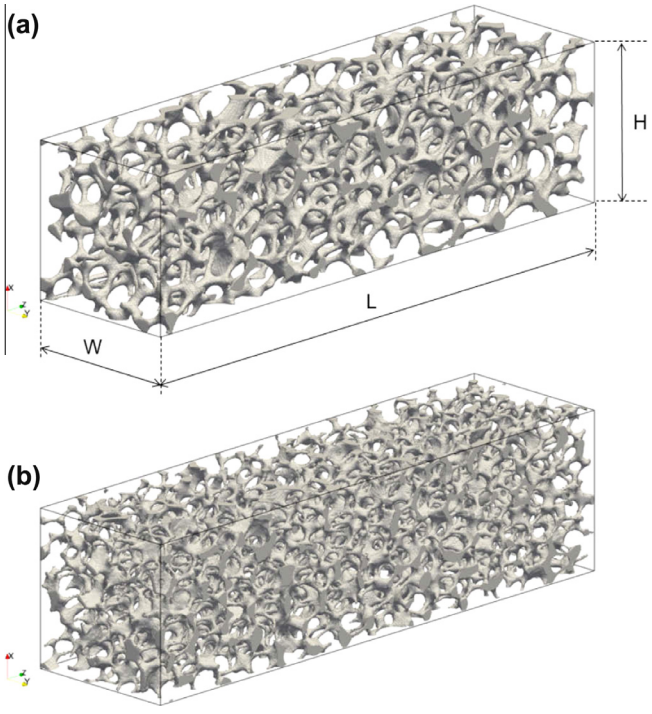

Fig. 1. 3D models of the samples used in this numerical study. (a) Sample 1, 10 nominal PPI. (b) Sample 2, 40 nominal PPI. Dimensions $W(Y) \times H(X) \times L(Z)$, $11 \times 11 \times 40$ mm.

2.1. Geometry

The mesh for the numerical simulations considers a rectangular cuboid of $11 \times 11 \times 40$ mm size (Fig. 1) extracted from 3D models of aluminium (Al 6101 T6) open-cell foams. The 3D models of the foams were obtained from micro-computed tomography (μ-CT) scans, a non-destructive method to generate accurate measurements of the internal structures of the sample [30]. Two samples with a similar porosity but different nominal pore density (10 PPI Fig. 1a, 40 PPI Fig. 1b) were selected for the studies. The relevant geometrical properties used to characterize the open-cell foam samples are: the solid fraction ($1-\varepsilon$), the thickness of the strut (t_s), the average diameter of the lateral face, or pore, of a single foam cell (d_p), the average diameter of the single foam cell (d_C), and the volumetric surface area (S_v). These values are summarized in Table 1. Details on the experimental techniques used by the authors to evaluate such properties and a clarifying magnification with the optical microscope highlighting cell, pore and struts can be found in a previous work which was more focused on the characterization of the supports [10].

For the simulation of the pressure drop and interphase heat transfer, the mesh consists only of the fluid phase, as negative of the solid matrix in Fig. 1. About 1.2 and 2.7 million control volumes, of which 74% are hexahedral, were used in the generation of the mesh of sample 1 and 2, respectively. For the simulation of the conjugated heat transfer, in contrast, the mesh has to be generated for both, the solid and the fluid phase. According to the different gap size in the studies, the range of the number of control volumes used for these simulations is between 1.6 and 2.3 million for sample 1 and 6.5–8.6 million for sample 2, with a fraction of hexahedral volumes of about 88%. More details about the mesh resolution, mesh independence of the solution and variations in grid size are reported in Section 4.3.

2.2. Governing equations

For the simulation of conjugated heat transfer the heat conduction equation is solved in the solid region, while mass, momentum, and energy conservation equations are solved in the fluid phase. The comprehensive general balance equations were implemented in conservative form for steady-state conditions. The mass conservation equation for the fluid phase is thus given by:

$$\nabla \cdot (\rho \vec{u}) = 0; \tag{1}$$

where ρ is the fluid density and u is the fluid velocity. The conservation of momentum, neglecting buoyancy effects, is given by:

$$\nabla \cdot (\rho \vec{u}\vec{u}) = -\nabla p + \nabla \cdot \vec{\tau}_{eff}; \tag{2}$$

where p is the pressure and $\vec{\tau}_{eff}$ is the effective viscous stress tensor, which includes turbulent viscosity if a turbulent model is selected.

Neglecting gravitational potential energy and internal heat generation, the equation of energy conservation for the fluid phase can be written as:

$$\nabla \cdot (\rho e \vec{u}) = -\nabla \cdot \vec{q}_{eff} - \nabla \cdot p\vec{u} - \nabla \cdot [\vec{\tau}_{eff} \cdot \vec{u}]; \tag{3}$$

where e is the internal energy per unit of mass and $\vec{q}_{eff}$ is the rate of heat addition to the fluid due to effective conduction, including the turbulent thermal conductivity if a turbulent model is selected.

The energy equation for the solid, without heat generation, is:

$$\nabla \cdot (k_s \nabla T) = 0; \tag{4}$$

where k_s is the thermal conductivity of the solid.

Table 1
Relevant geometric properties of the investigated foam samples.

	$1-\varepsilon$	S_v (m^{-1})	d_c (mm)	d_p (mm)	t_s (mm)	d_h (mm)
Sample 1	10.3%	649	3.58	1.85	0.39	5.53
Sample 2	11.0%	936	2.45	1.29	0.31	3.80

As stated above, different flow regimes were explored in the simulations. Defining a Reynolds number based on the pore diameter and the interstitial bulk velocity, four different regimes can be identified [31]: Darcian creeping flow ($Re \leqslant 1\sim10$), Forchheimer flow ($1\sim10 < Re \leqslant 150$), post-Forchheimer unsteady laminar flow ($150 < Re < 300$) and fully turbulent flow ($Re > 300$). As a consequence, for simulations with Reynolds numbers higher than 300 (here: in the range of 1E+3–1E+4) a Reynolds averaged Navier–Stokes (RANS) based turbulent model is used. Among the available RANS models, the shear-stress transport (SST) k-ω model was selected because it is considered more flexible for wall bounded flows as it includes a blending function to ensure that the model equations behave appropriately in both the near-wall and far-field zones [32].

Two different fluids are considered in the simulations: air and water. For air the equation of state for an ideal gas is applied, while for the simulations with water the fluid is considered incompressible, but density variation due to temperature effects is included in the formulation. All the simulations are performed in the subsonic regime (Mach number <0.3). The effect of temperature variation is also considered in the calculation of the viscosity, implementing the Sutherland [33] model for air and a polynomial dependency for water. The other thermophysical properties are assumed constant and are calculated for the average temperature of the system.

2.3. Boundary conditions

Different boundary conditions are considered in the simulations, according to the specific fluid dynamic cases or thermal parameters investigated.

2.3.1. Pressure drop simulations

For the pressure drop calculations, the flow direction is fixed in the *Z*-axis and the standard set of Dirichlet boundary conditions for the inlet velocity and outlet pressure is imposed. No-slip boundary conditions and zero gradients for the pressure field are imposed at the interface with the solid foam. The external wall is not considered and therefore symmetric boundary conditions are applied at both the *Y*-axis and *X*-axis faces. The fluid properties are calculated at 300 K.

2.3.2. Interphase heat transfer simulations

For the evaluation of the interphase heat transfer, the reconstructed 3D model is supposed to represent a volume deep inside the reactor bed. Thus, no external walls are considered and similar boundary conditions as for the case of pressure drop simulations are applied for velocity and pressure. An external contribution to the energy equation is directly applied at the interface between the open-cell foam and the fluid. This contribution is implemented in the form of a constant heat flux, increasing the temperature of the fluid which enters at 300 K. The case of a fixed heat flux was found to be more representative of a real case than a case study with fixed solid temperature [34]. To preserve the assumption of constant thermal conduction, the maximum increase of the fluid temperature was kept below 2 degrees for water simulations and 10 degrees for air simulations.

2.3.3. Conjugated heat transfer simulations

In contrast to the previous simulations, for the case of conjugated heat transfer the computational mesh also includes the solid phase. Moreover, the effect of the wall coupling is explicitly investigated in detail. For this reason, the mesh was changed accordingly in order to consider a wall on the bottom face of the *X*-axis. Three different scenarios of physical coupling were considered:

(1) Direct contact with the solid matrix;
(2) Gap of 100 μm;
(3) Gap of 1 mm.

Since the mesh height is kept constant, the solid matrix is shifted in X direction, as can be seen in Fig. 2. The examples of sample 1 presented in Fig. 2 show the effect of the gap on the velocity field (Re = 50). There is almost no difference between case 1 and 2 (Fig. 2a and b), while for the larger gap of case 3 (1 mm, Fig. 2c), the near wall region becomes a preferential bypass for the fluid flow.

In order to represent a fully developed flow a pressure drop is imposed in the flow direction (*Z*-axis) as proposed in literature [34,35]. For this, the result of the pressure drop simulations served as input data. No-slip boundary conditions are now applied also at the bottom face of the *X*-axis, which represent the external wall. To allow heat transfer between the two phases, at the fluid–solid interface continuity of the heat flux and equal surface temperature is imposed [34]. The heated surface is now located at the inner wall, while the fluid entrance temperature is 300 K.

Two different cases are considered at the inner wall surface: fixed temperature and fixed heat flux. The first case is applied for air and water simulations with direct contact between the mesh of the open-cell foam and the wall face and for the case of a 100 μm gap, respectively. The second case is used only for selected simulations with air (for all three cases, i.e., direct contact, 100 μm gap, and 1 mm gap), in order to compare this condition with the simplified case of an adiabatic boundary condition between the foam solid phase and the wall. Moreover, the additional case of physical contact between the wall and the solid phase while assuming a thermal discontinuity (i.e., adiabatic boundary conditions), is simulated for air. This set of simulations allows for evaluating the validity of such simplified approximations which are common for simulations of conventional packed beds of spherical particles.

3. Results

The simulations were run on the "lima cluster" of the High Performance Computing Center of the University of Erlangen-Nürnberg (Regionales RechenZentrum Erlangen, RRZE). A second order upwind scheme was used for the convective calculations in the turbulent regime and for the conjugated heat transfer simulations, while a linear scheme was used in the other cases. The pressure field is solved with the semi-implicit method for pressure-linked equations (SIMPLE). The simulations were stopped when the normalized residual for continuity, energy and momentum equation dropped below 10^{-6}.

3.1. Pressure drop

The pressure drop was evaluated by simulations of fluid flowing through the open-cell supports in order validate the implemented CFD model for the whole range from laminar to turbulent conditions. The general trend of the pressure drop increasing as function of increasing velocity was found in reasonable agreement with literature data and models [1]. However, no literature model is recognized to be generally valid, with reported standard deviations as

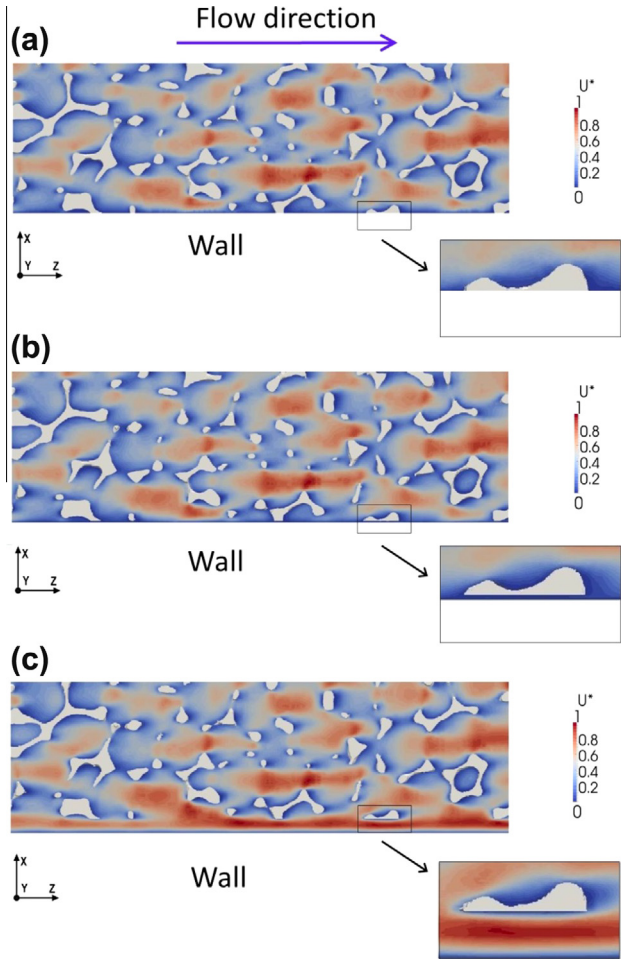

Fig. 2. Distribution of the dimensionless velocity component in flow direction ($U^* = U_Z/U_{Z,Max}$) in a longitudinal section (*Y*-axis normal) of the 3D model of sample 1 for different wall coupling scenarios. (a) No gap; (b) 100 μm gap; (c) 1 mm gap. Re = 50.

high as 100%. For the comparison in this work, an empirical general correlation, recently proposed for metallic and ceramic open-cell foams [36], was selected. In Fig. 3, the results from simulations are presented in dimensionless form (Reynolds number vs. Hagen number and hydraulic pore diameter) showing the same trend as the literature correlation, while deviations up to 60% can be observed depending on the specific case.

The pressure drop can be expressed as sum of viscous and inertial terms, such as in the Forchheimer equation for flow in porous media:

$$\frac{\Delta p}{\Delta L} = \frac{\mu}{K}u + \frac{F}{\sqrt{K}}\rho u^2; \tag{5}$$

where K is the Darcian permeability and F is the Forchheimer inertial coefficient.

The values for the coefficients K and F are assumed to be a function of the geometrical characteristics of the bed only, and they can be calculated as result of best fitting interpolation (i.e., minimizing the sum of the square of residuals between the results from simulations and pressure drop per unit length as function of a second order polynomial of velocity). The resulting values are presented in Table 2, showing a reasonable agreement with those calculated using an empirical literature correlation [37].

3.2. Interphase heat transfer

The average interphase heat transfer coefficient (h_i, W m^{-2} K^{-1}) is calculated for each simulation as:

$$h_i = \frac{\int\int_S \frac{qdS}{(T_x - T_{b,Z})}}{\int\int_S ds}; \tag{6}$$

where q is the specific heat flux at the fluid-foam interface and S is the surface of the open-cell foam. The bulk temperature (T_b) is defined as the average temperature weighted by the mass flow ($u_n{*}\rho$) crossing a section of fluid (Γ_z) normal to the axial coordinate (Z):

$$T_{b,Z} = \left.\frac{\int\int_\Gamma T_f u_n \rho d\Gamma}{\int\int_\Gamma u_n \rho d\Gamma}\right|_Z; \tag{7}$$

The results for the interphase heat transfer coefficients are presented in Fig. 4, for both samples and fluids, as function of the dimensionless velocity (i.e., Reynolds number). The dimensionless heat transfer coefficient itself is presented as the ratio between Nusselt number and the one-third power of the Prandtl number, to plot the results of both air and water simulations.

Different models are proposed in literature to predict the interphase heat transfer coefficients [16,37–39], but in general a wide variation of experimental literature data around the fitting correlations can be observed (> 40% [40]). The reason for this is mainly connected to the irregularity in the geometrical properties of the commercial foam samples such as, e.g., distribution of pore sizes and cross section diameters or closed cells. For comparison purposes, a simplified literature correlation [39] is used as reference in Fig. 4. In order to be consistent with the present paper, the original correlation was modified to use the pore diameter as characteristic length, based on the geometrical relation of the cubic cell model [15]. The graph of Fig. 4 proves that the results of the description of the heat transfer in the numerical study are consistent with literature data.

3.3. Conjugated heat transfer

According to the specific boundary conditions, the average overall heat transfer coefficient (U, W m^{-2} K^{-1}) is calculated in

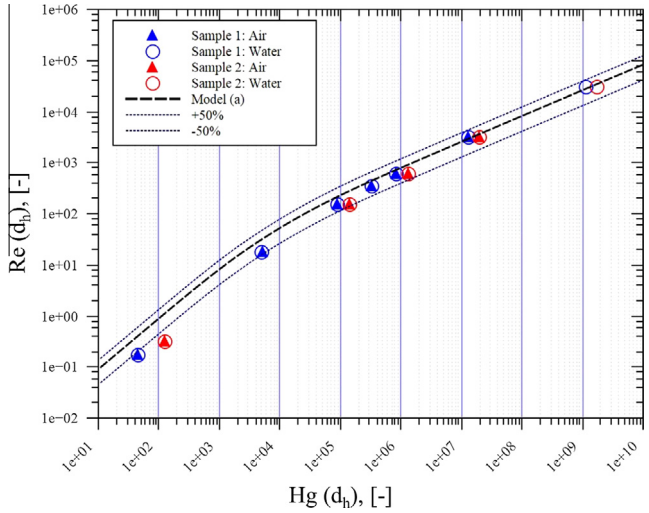

Fig. 3. Simulation results of dimensionless velocity (Reynolds number) and correspondent dimensionless pressure drop (Hagen number) compared with a general correlation (a: [36]) for pressure drop in both ceramic and metal open-cell foams.

Table 2
Viscous and inertial coefficients calculated from the simulations compared with those calculated with literature correlation.

	K (m^2)	F (m^{-1})	K^a (m^2)	F^a (m^{-1})
Sample 1	1.2e-7	3.8e-2	7.4e-8	4.1e-2
Sample 2	4.5e-8	3.7e-2	4.6e-8	4.4e-2

[a] Literature model [37].

two different ways. If a fixed heat flux is imposed on the heated surface, the coefficient is calculated according to Eq. (8):

$$U_q = \frac{\int\int_A \frac{q}{(T_W - T_{bZ})} dA}{\int\int_A dA}; \tag{8}$$

where q is the specific heat flux and A is the surface of the heated wall. On the other hand, for the simulations where a fixed temperature is applied on the external wall, the overall heat transfer is instead calculated as given in Eq. (9):

$$U_T = \frac{\int\int_A q dA}{\int\int_A dA} \frac{1}{\Delta T_{lm}} \tag{9}$$

where ΔT_{lm} is the log mean temperature difference, calculated as:

$$\Delta T_{lm} = \frac{\Delta T_{out} - \Delta T_{in}}{\ln(\Delta T_{out}/\Delta T_{in})}; \tag{10}$$

In Eq. (10) ΔT_{in} and ΔT_{out} are the temperature differences between the inlet or the outlet fluid average temperature and the fixed temperature of the wall. The results for the overall heat transfer coefficient for the simulations with air and water are shown in Fig. 5, for both sample 1 (a) and sample 2 (b), as function of the pore Reynolds number. In general, the overall heat transfer coefficient is dependent on the heat transfer properties of both the solid and the fluid phase. In our simulations, the 3D models are based on specimens with nearly identical solid fraction and thus also very similar effective thermal properties of the solid phase, as confirmed in a previous characterization [10]. For this reason, the relative differences of the overall heat transfer coefficient calculated for each run must be related to the fluid phase or to the different boundary conditions applied at the wall interface.

3.3.1. Effect of wall coupling

Focusing on the simulations with air, three cases can be distinguished with regard to the analysis of the thermal coefficient. The first case is the one presenting the lowest thermal coefficient at same Reynolds numbers, i.e., the configuration corresponding to the maximum gap size (1 mm). Then, the second case comprises a group of data composed by the two investigated cases with a gap size of 100 μm, i.e., with fixed heat flux or fixed temperature, and the simplified model with no heat flux (adiabatic) at the interface between the wall face and the solid phase mesh. This group results in a slightly higher overall coefficient than the previous case. However, the difference tends to decrease with increasing Reynolds numbers, as can also be observed for other kinds of structured packings such as, e.g., cross flow structures [41]. As can be seen in Fig. 5, the ratio of the overall heat transfer coefficients for the cases with fixed heat flux at 100 μm and 1 mm changes from a factor of 2.2 (for sample 1), or 3.5 (for sample 2), to about 1 when changing from the lowest to the highest investigated velocity.

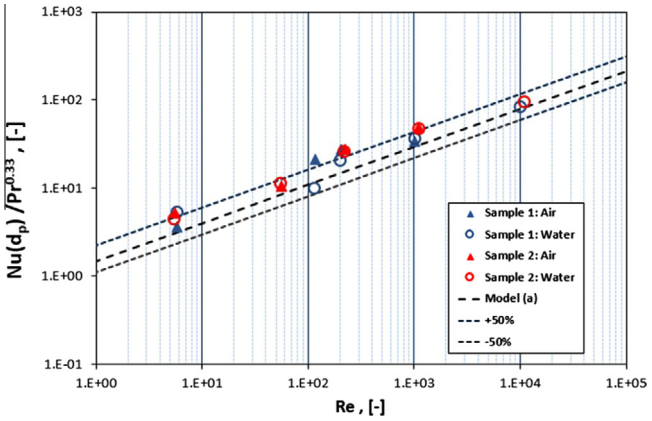

Fig. 4. Simulation results of dimensionless interphase heat transfer coefficient (ratio between the Nusselt number based on average strut cross section and Prandtl number) and correspondent dimensionless velocity (Reynolds number based on average pore diameter) compared with a literature correlation [39].

Some preliminary conclusions can be inferred from the simulations with thermal discontinuity between the open-cell foam mesh and the inner wall face. The thermal overall coefficients of the air simulations with adiabatic boundary conditions are closer to the ones with 100 μm gap and higher than those with 1 mm gap. This suggests that, for the studied cases, the area of the open-cell foam mesh normal to the wall inner surface (the potential area of direct contact) has no impact on the thermal performance if there is no thermal continuity between the solid phase of the open-cell foam and the wall. Instead, the heat transfer is partially affected by the thermal conductivity of the fluid and the thickness of the gap. This explains the lower values of the overall thermal coefficient for simulations with 1 mm gap and the decreasing difference between the water (i.e., a highly conductive fluid) simulations with or without gap.

The largest values (case 3) are obtained when the solid phase is thermally directly connected with the wall. As example, Fig. 6 shows the temperature scale of the flow stream and the solid mesh (sample 1) for the two cases of fixed wall temperature directly applied to the solid phase or with a gap of 100 μm. The normalized temperature is in the higher 20% for the case of direct wall-solid contact and in the lower 40% for the case of a gap. In fact, the overall heat transfer coefficient in the case of fixed wall temperature is in average 7.4 times higher than the corresponding value for the case of a 100 μm gap (see Fig. 5). Of course, this result is expected and connected to the lower thermal resistance for the heat flux moving directly inside to the highly conductive solid matrix. Nevertheless, for this configuration, the case with Dirichlet boundary conditions exhibits a coefficient larger than that for the case with Neumann boundary conditions. This could also be related to the different procedure of thermal coefficient evaluation (Eq. (8) vs. Eq. (9)). Similar considerations are valid for the simulations with water as fluid. However, here the difference between the cases with or without the gap is less prominent, the values decrease from a factor of 2 to 1 in the range of explored Reynolds numbers. This clearly points out the significant impact of the used boundary condition at the wall skin in the modeling of the real performance of open-cell foam packed reactors. More generally speaking, this impact is not only important for the investigated cases here, but also for other heat transfer literature studies where coefficients are often reported for only one specific boundary condition (which sometimes is even not explicitly stated).

3.3.2. Effect of the fluid thermophysical properties

From Fig. 5 it can clearly be seen that at the same Reynolds number the heat transfer coefficient in runs with a fluid representing water properties is about one order of magnitude higher than the corresponding ones with air. In particular, it is about 11 times higher for the simulations with direct contact between the wall and the solid matrix, and an average ratio of about 41 times higher for the case of a 100 μm gap.

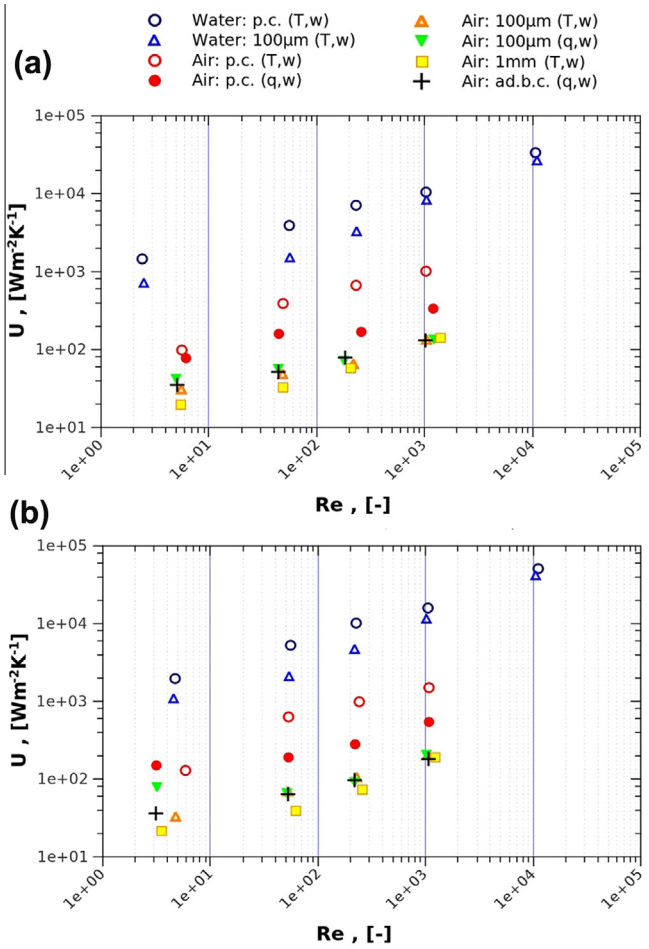

Fig. 5. Overall heat transfer coefficient for sample 1 (a) and 2 (b) as result of different open-cell foam and wall coupling and air or water as fluid: perfect contact (p.c.), adiabatic boundary condition (ad.b.c.), gap of 100 µm or 1 mm, fixed temperature (T,w) or fixed flux (q,w) on the heated surface.

3.3.3. Effect of velocity

Increasing the velocity has a positive effect in all the configurations studied. However, while the Reynolds number increases about 3 orders of magnitude for air and 4 for water, the overall heat transfer coefficient only increases about one order of magnitude. This effect is more important for the simulations considering a gap close to the wall. For example, the simulations for air with a 1 mm gap intersect the ones with a 100 µm gap, and the simulations with a 100 µm gap for water even intersect those with the direct wall-solid coupling.

3.3.4. Effect of foam geometry

For each of the investigated wall coupling scenarios, the trend as a function of the Reynolds number is similar for both the samples. However, the absolute value of the overall heat transfer coefficient is higher for sample 2 (i.e., an average increment of about 40%). At this point it is worthy of note that the two 3D models were derived from samples with similar porosity, but different pore density. As sample 2 features a higher pore density, it means that decreasing the size of the pore or strut diameter (i.e., increasing the specific surface) has a positive effect on the resulting overall heat transfer coefficient.

4. Connection between overall and local thermal properties

In the previous Section 3.3 the 1D heat transfer coefficient derived for each numerical test was analyzed. It is obvious that this coefficient is not more than a lumped parameter, representing the overall effect of the micro scale and near wall heat transfer [42]. In contrast to this traditional approach (and in contrast to most experimental set-ups), the simulations performed in this work allow for the identification of the individual contributions of solid, fluid, and interphase heat transfer. Therefore, the aim of this paragraph is to separately investigate the wall heat transfer coefficient in order to derive empirical correlations according to the specific wall coupling scenario. Since the transversal temperature gradient is much higher than the axial one, the contribution of the axial effective conductivity is neglected. In fact, the uncertainty due to this approximation, estimated with a general criterion derived for heat transfer in packed beds [43], was found important only for the simulation at the lowest Reynolds number (less than 1% already for the simulations with air at Reynolds numbers higher than 100 or water as fluid, assuming an axial effective conductivity of the same order as the radial one).

4.1. Case of thermal continuity between the wall and the solid matrix

When open-cell metallic foams are used as compact heat sinks they are usually directly brazed to a base plate. For this scenario, different authors attempted to describe the heat transfer in

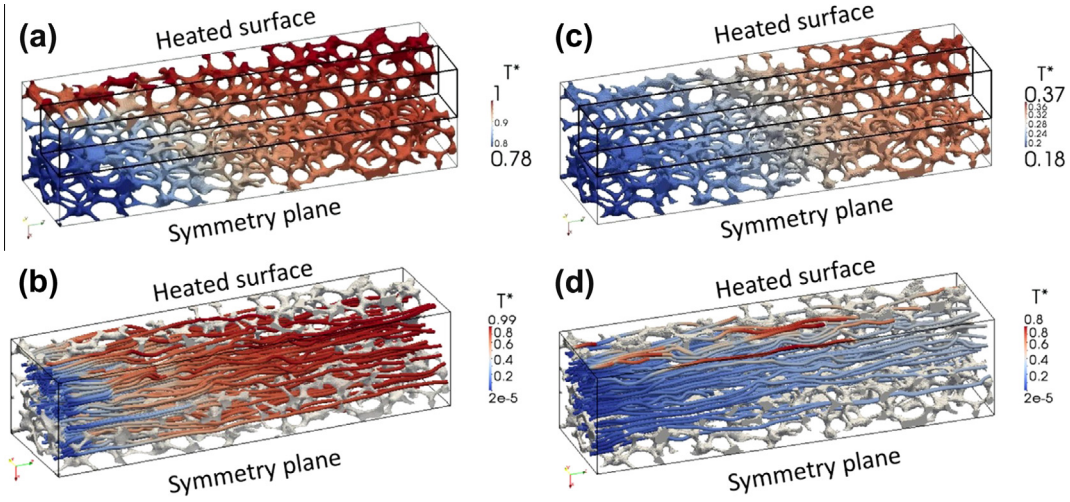

Fig. 6. Temperature distribution $[T^* = (T - T_w)/(T_{inf} - T_w)]$ in simulations of conjugated heat transfer for sample 1. Cases of fixed wall temperature directly applied to the solid phase (a and b) or with a gap of 100 µm (c and d). Solid phase: a and c. Fluid streams: b and d.

resemblance to the conventional approach for finned surfaces [44–46]. For example, assuming a repetitive simple cubic structure for the foam matrix with adiabatic tip, Ghosh [45] proposed to correct the standard fin efficiency (η_F), accounting for the cross connections in the foam filaments, while the cross connections itself are considered as additional fins, affected by an efficiency factor, too ($\eta_{½}$):

$$\eta_F = \frac{\tanh\,(MH)}{(MH)};\quad M = m\sqrt{(1+4\eta_{1/2})};$$
$$\eta_{1/2} = \frac{\tanh\left(m\frac{d_p}{2}\right)}{\left(m\frac{d_p}{2}\right)};\quad m = \sqrt{\frac{4h_i}{k_s t_s}}; \tag{11}$$

Following this approach, the overall heat transfer efficiency is the result of the contribution of the heat flux through the extended surface and the heat transfer from the unfinned base (h_U). Using this foam efficiency and the average fluid temperature, the overall heat transfer coefficient weighted on the base surface can be calculated according to Eq. (12) [47]:

$$U = \eta_F h_i S_v H + h_U \varepsilon;\left(\frac{A_F}{A} = \frac{LWS_vH}{LW};\ \frac{A_U}{A} = \frac{LW\varepsilon}{LW}\right); \tag{12}$$

The geometrical parameters are a consequence of using the base surface as reference area. The second term on the right side of Eq. (12) is often neglected because the bare base area is usually much smaller than the one of the extended surface. Moreover, even when this contribution is taken into account the same convective coefficient is used for both the extended surface and the base. Based on this assumption, the overall heat transfer coefficients calculated with Eq. (12) are shown in Fig. 7 in comparison with the values derived from the simulations. The data (hollow symbols) of sample 1 and 2 are displayed for both air and water simulations for the cases with fixed temperature or fixed heat flux on the heated base. However, the use of the interphase heat transfer coefficient [39] also on the unfinned base results in an overprediction of the overall coefficient.

On the other side, using electrical analogy, the equivalent thermal resistance can also be written as sum of the phase contributions as in Eq. (13) [42]:

$$\frac{1}{R_e} = \frac{1}{R_{f,e}} + \frac{1}{R_i + R_{s,e}}; \tag{13}$$

where the equivalent thermal resistances are inversely proportional to the corresponding effective thermal coefficients: $R_e \propto \frac{1}{U}$, $R_{f,e} \propto \frac{D_h}{k_{f,e}}$, $R_i \propto \frac{A-A_U}{h_i S}$ and $R_{s,e} \propto \frac{D_h}{k_{s,e}}$.

Thus, the wall heat transfer coefficient between the fluid and the bare surface can be assessed distinguishing the values of solid and interphase heat transfer resistances. In fact, the effective solid conductivity of the reticulated samples in our simulations can be predicted with a literature model [48], as established in a previous study [10]. The interphase heat transfer coefficient can in turn be estimated as shown in Section 3.2. The positive residual is the contribution connected with the fluid phase. It can be either considered negligible for air simulations (or gas in general), or, in contrast, it can be the determinant contribution for highly conductive fluids such as, e.g., in the simulations with water. In this case, the Nusselt number based on the estimated unfinned convective coefficient has been correlated with a power law of the Reynolds number (based on d_p for both the dimensionless numbers), resulting in an exponent of 0.52 and pre-multiplicative constants of 0.81 and 0.93 for sample 1 and 2, respectively.

As a result, the overall heat transfer coefficients were recalculated replacing in Eq. (12) the estimated value of the fluid thermal coefficient. The new coefficient values reveal a reduced margin with the simulation data as can be seen in the parity plot of Fig. 7 (filled symbols).

4.1.1. Adaptation for heterogeneous catalytic supports

In an equivalent electric resistance scheme, the interphase resistance can be placed in series with the solid or with the fluid effective conductivity. The first case, the same as in the network of Eq. (13), is more effective when the open-cell foam is used as heat exchanger. In contrast, when the structure is used as catalytic support the most relevant temperature is the one on the surface of the catalyst where the reaction takes place. Therefore, it is more appropriate to account the interphase thermal resistance in series with the effective conductivity of the fluid phase. Thus, Eq. (13) has to be modified to:

$$\frac{1}{R_e} = \frac{1}{R_{f,e} + R_i} + \frac{1}{R_{s,e}} \tag{14}$$

It is worth mentioning that the same networks of Eqs. (13) and (14) are obtained for unconsolidated packed beds when the two limiting cases are high or low flow rate conditions [42]. In any case, three different physically relevant regimes can be identified, where only one among interphase, fluid, or solid thermal effective conductivity is dominant. Therefore, it is reasonable to define two dimensionless parameters to take into account the solid and fluid effective conductivity, and the interphase heat transfer coefficient:

$$k = \frac{k_{s,e}}{k_{f,e}};\ \text{and}\ Nu_{e,i} = \frac{h_i (D_h/2)^2 S_v}{k_{f,e}}; \tag{15}$$

The boundary between each region depends on the ratio of these parameters and geometrical constants [49]. However, for metallic open-cell supports only two cases are relevant. If the fluid is a gas, k is generally much greater than 1, and this results in the physical case where the solid effective conductivity is the dominant contribution. If the fluid is a liquid, with increasing Reynolds number k could become lower than 1, but usually $Nu_{e,i} > 1$, which means that it falls in the physical regime where the fluid effective conductivity is dominant.

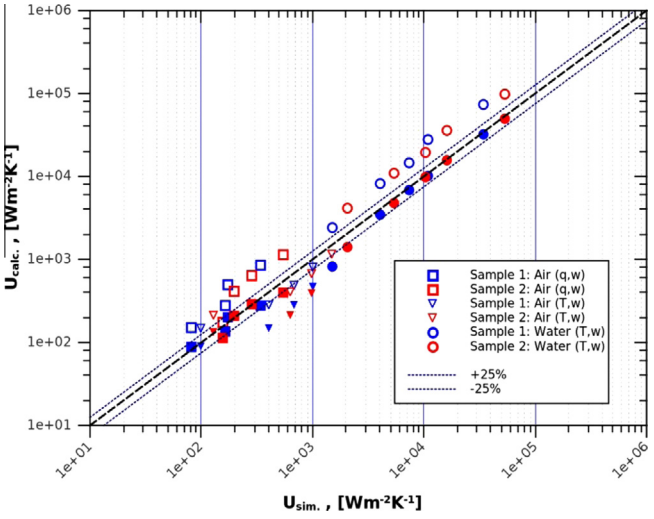

Fig. 7. Parity plot between overall heat transfer coefficients estimated from the simulations and the values calculated according to Eq. (12). Open symbols: $h_U = h_i$. Solid symbols: $h_U \neq h_i$.

4.2. Case of thermal discontinuity between the wall and the solid matrix

When the solid foam matrix is not directly coupled with the wall, the additional resistance of the near wall region must be added in series to the bed effective conductivity. With a pseudo-homogeneous approach, the effective heat transfer coefficients in tubular geometries can be calculated from the measurements of the wall and the central axis temperature profiles [50], using a truncated series of first kind Bessel functions. In a similar way, the wall heat transfer coefficient can in a first approximation be estimated from the present simulations. The results were found virtually equivalent to those calculated with the literature relation between 2D and 1D thermal parameters [51,52], i.e., subtracting the effective bed conductivity calculated as in Eq. (13) from the overall heat transfer coefficient. For this reason, this approach was used to derive the wall heat transfer coefficients for all the simulations with thermal discontinuity between the solid matrix and the heated wall.

The results for the simulations with a gap size of 100 μm are presented in dimensionless form in Fig. 8. The Nusselt numbers are related to the simulations of fixed wall temperature with water and air for both, sample 1 and sample 2, and are plotted as function of the Peclet numbers. The characteristic length used here is the pore (window) diameter in consistency with the common approach for packed beds. This was done in order to account for the different thermal properties of the two different types of fluids investigated.

On the basis of the simulations for the case of constant wall temperature and 100 μm gap a best fitting correlation, Eq. (16), is derived consisting of a static and a dynamic term.

$$Nu = 1.97 + 0.09\ Pe^{0.73};\ 2 < Pe < 6.4\,E+4; \tag{16}$$

It is worth noticing that Eq. (16) reasonably predicts even the wall coefficients of the simulations for the foam-wall adiabatic BC (also reported in Fig. 8), despite the fact that this data was not included in the derivation of the correlation coefficients. In fact, for both cases with foam-wall adiabatic BC and 100 μm gap, the deviation between the wall heat transfer coefficients evaluated from the simulations or from Eq. (16) is below 25%, except for the data at the lowest flow rates where the sensitivity to the measured temperature is higher, and thereby also the impact of the different wall thermal boundary conditions.

The simulation results for the case of constant wall heat flux and 100 μm gap size, on the other hand, could be fitted by the following Eq. (17):

$$Nu = 3.52 + 0.02\ Pe^{0.88};\ 2.2 < Pe < 829; \tag{17}$$

In an analogous manner, a correlation is also proposed for the simulations with a 1 mm gap and constant wall temperature. The dependency on the Peclet number is kept the same as in Eq. (16), while the static contribution is subject to re-assessment and fitting. This approach was chosen since according to Fig. 5 the overall coefficients of simulations with air at 100 μm, 1 mm, and adiabatic B.C. converge with increasing Peclet number. The resulting correlation is given in Eq. (18):

$$Nu = 0.91 + 0.09\ Pe^{0.73};\ 2.2 \leqslant Pe \leqslant 749; \tag{18}$$

The wall heat transfer coefficients for the simulations with a 1 mm gap and values calculated by Eq. (18) are presented in Fig. 9 in terms of Nusselt and Peclet numbers. The difference between the coefficients derived from the simulations and those calculated with Eq. (18) remains in the region of 25%.

The dynamic contribution, which is a function of the Peclet number, shows the same dependency on the flow rate and fluid properties, at least in the range of conditions explored in this study. Instead, the main effect of the gap size is connected with the static contribution to the wall heat transfer coefficient. In particular, when increasing the distance between the solid matrix and the wall, the static contribution decreases. However, this coefficient is not directly proportional to the thickness of the gap, which changes by a factor 10. This suggests that with a gap size of 1 mm, the pure mono-directional conductive description of the near wall heat transfer is sufficient, but more detailed analysis at different gap sizes is required.

4.2.1. Comparison with literature correlations

As already mentioned in the Introduction, only few publications are available in literature for comparison of the wall heat transfer coefficients estimated in this numerical study. In particular, we are aware of only two published correlations for the wall heat transfer coefficient in channels filled with open-cell foams [17,21]. In both studies, the correlations are derived from thermal experiments with gas flow in the laminar regime, and therefore their applicability is limited. The first correlation was derived on the basis of the results collected with air for one single 30 PPI Al_2O_3 foam of 87% porosity [17], and it considers only the convective contribution. The wall Nusselt number is linked to a power law of the Reynolds number, and both the dimensionless numbers are based on the inverse of the specific surface area as characteristic length. In the second work [21], instead, the wall heat transfer coefficients are estimated from temperature profiles collected over five metal foam samples in the range of 10–40 PPI and 90–95% porosity, using gas (N_2, He) as fluid. The Nusselt number based on the wall heat transfer coefficient and the cell diameter is modeled as the sum of a static and a dynamic contribution, and the static contribution was dominant in the explored range of flow rates. The dynamic part is instead related with a power law to the Reynolds number.

Different levels of agreement are found between the wall heat transfer coefficients predicted with these literature correlations and those derived in the present study. When focusing on the cases with air and using the first correlation [17] and a specific surface calculated according to the reference, the absolute average deviation has a minimum value of 24% in simulations with 100 μm gap and fixed temperature and a maximum of 33% in the simulations with 1 mm gap.

In order to compare with the present results, instead, the second correlation [21] can be rephrased in terms of foam pore size as characteristic dimension, assuming an average cell to pore size ratio of 2.23 [53] and Pr = 0.72, thus obtaining:

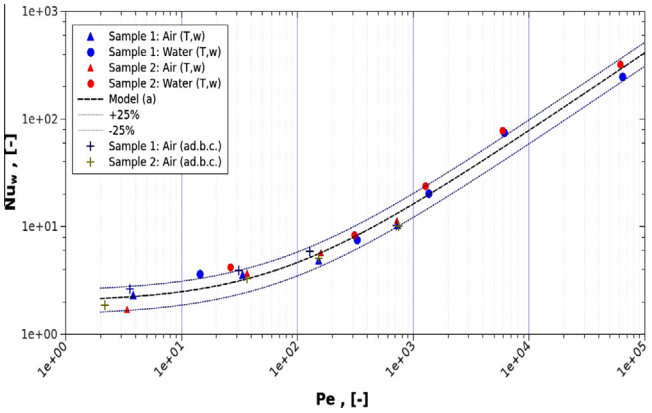

Fig. 8. The wall heat transfer coefficients with air and water simulations estimated for the cases with gap size of 100 μm and adiabatic BC (ad.b.c.) with fixed temperature (T,w) on the heated base. (a) Correlation proposed in this work, Eq. (16). The data are shown in dimensionless form as Nusselt and Peclet numbers based on the pore size as characteristic length.

$$Nu = 3.22 + 0.019\ Pe^{0.8};\ 1.25 < Pe < 80; \quad (19)$$

The structural similarity with Eq. (17) for the case of 100 μm gap (the same gap value was postulated but not measured by the authors in [21]) is evident, whereas in quantitative terms the deviation of the static term is −8.5%.

However, when the same correlations are applied to the water simulations (i.e. high Pe numbers), the average error increases up to 77% and 59%, respectively. The reason for this is that the correlation in [21] was developed based on experiments using gases as working fluids, featuring a Prandtl number eight times smaller.

4.2.2. Controlling radial thermal resistance

Defining for both the overall and the wall heat transfer coefficient a Biot number based on the effective conductivity of the foam bed $\left(Bi\ (U) = \frac{UD_h}{k_e};\ Bi\ (h_w) = \frac{h_w D_h}{k_e};\right)$ the two of them can be related as $Bi\ (U) = \frac{\xi Bi\ (h_w)}{\xi + Bi\ (h_w)}$, where ξ is a correcting coefficient in the range of 6–8, depending on the reference [42]. It can easily be seen that the overall Biot number is bounded between the two limiting cases: $Bi\ (U) \approx Bi\ (h_w)$, $Bi\ (h_w) \to 0$, and $Bi\ (U) \approx \xi$, $Bi\ (h_w) \to \infty$. Otherwise, by defining an arbitrary relative error α $(0 < \alpha < 1)$, it is possible to identify the cases where only one out of the wall and the bed heat transfer coefficients must be taken into account:

$$Bi\ (h_w) \leqslant \alpha\xi \ \rightarrow\ U \cong h_w (err. = \alpha);$$
$$Bi\ (h_w) \geqslant \frac{\xi}{\alpha} \ \rightarrow\ U \cong \frac{k_e}{D_h}\xi (err. = \alpha); \quad (20)$$

4.2.3. Comparison with unconsolidated packed beds

Also for the case of conventional fixed bed reactors of random packings the wall heat transfer coefficient is calculated by well-established correlations as the sum of a stagnant and a dynamic contribution [54]. The static contribution is constant and it is controlled by the gas thermal conductivity as the bed porosity is reasonably close to 40% in typical applications. The dynamic contribution is connected to the flow rate, and it shows a strong positive dependency on the Reynolds number. In case of low conductive fluids (e.g., gas and oxidative atmosphere) or low flow rates, the convective transfer mechanism collapses. As this is, however, the main contribution to packed bed heat transfer coefficients, in such conditions this reactor technology is limited and unfavourable. Instead, in the same conditions the heat transport using open-cell foam beds is superior, because the heat conduction is still effective. As example, the overall heat transfer coefficient of a tubular reactor with a pellet or a foam packing can be compared for the oxidation of methanol to formaldehyde using Fe and Mo oxide catalysts [55]. The properties of the foam packing have been selected according to a commercially available open-cell foam (40 PPI, 85% porosity, Aluminium) similar to the sample considered in this study but with greater relative density to enhance the effective radial thermal conductivity. The wall heat transfer coefficients are similar, but higher for the case of the foam packed reactor (310 vs. 275 W m^{-2} K^{-1}). Thus, the overall effective conductivity depends on the effective thermal conductivity of the support. As the open-cell foam features an effective radial conductivity one order of magnitude higher than that of the random packing (~10 vs. 1 W m^{-1} K^{-1}), the overall heat transfer coefficient is about 50% higher.

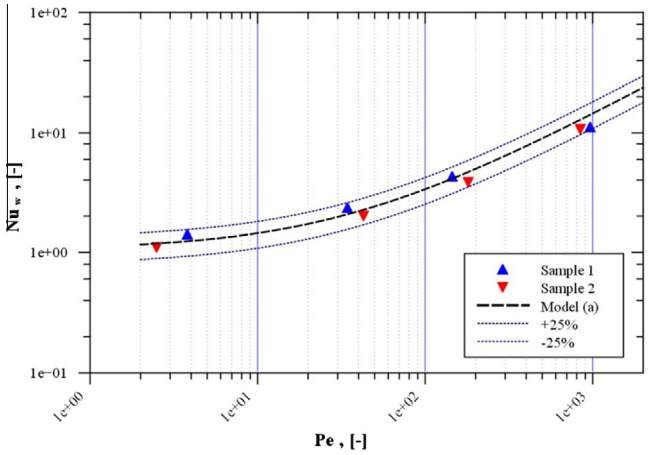

Fig. 9. The wall heat transfer coefficients estimated for the air simulations of sample 1 and 2 and a gap size of 1 mm. (a) Correlation proposed in this work, Eq. (18). The data are shown in dimensionless form as Nusselt and Peclet numbers based on the pore size as characteristic length.

4.3. Source of error

In the finite volume analysis the resolution of the mesh grid has a crucial impact on the quality and reliability of the results. For this reason, the final meshes used in the simulation studies were checked to be consistent with the geometrical properties of the original samples. The relative errors between the 3D model and the data measured with micro-computed tomography are smaller than 3% for the specific surface and smaller than 0.4% for the porosity. On the other side, in laminar simulations, the flow field was compared for grids with different resolution. According to a literature approach [56], the error in the evaluation of the interphase and overall heat transfer coefficients connected with the use of the finest mesh has been estimated to be about 4%. Moreover, to minimize the impact of inlet, length and exit effects, a sensitivity analysis was carried out. In particular, the thermal coefficients were calculated also for the case of a shortened volume, removing a section of 5 mm, which corresponds roughly to 3–4 pore diameters for sample 1 and 2, respectively, at the inlet and at the outlet of the 3D model. The average variations in the estimated coefficients is found to be below 3%, except for the case of conjugated heat transfer simulations with air at the lowest flow rate (Re < 10), where the average variation of the overall heat transfer coefficient reaches the peak of 39%. That way, it could be proven that the structure of the open-cell foam reduces the boundary effects to a region of only a few pore diameters.

5. Summary and Conclusion

Within the framework of the characterization of the effective thermal properties of metal open-cell foams as novel and enhanced supports in catalytic reactors, the focus of this study is the effect of the gap size between the foam and the reactor wall on the wall heat transfer coefficient. In order to close the knowledge gap regarding suitable data and correlations in open literature, a systematic numerical study was performed for an in-depth investigation of the influence of the coupling between the solid phase of the structured support and the reactor wall.

The numerical approach allowed overcoming the limits of conventional experimental facilities by also exploring the range of high Reynolds numbers up to the turbulent regime, and also by considering different fluid properties such as air (Pr = 0.7, STP) and water (Pr = 5.8, STP). Two different geometrical models, generated from scanning of real samples of 10 and 40 PPI by micro-computed tomography, were used in this study. The validity of the numerical model has been proved by comparing the calculated results of independent simulations for pressure drop, interphase, and conjugated heat transfer with available literature correlations. Nevertheless, the present lack of experimental data suitable for

extensive validation of the results of this modeling study for the whole explored range of operation conditions suggests the necessity to further continue the analysis, especially on the experimental side.

The overall heat transfer coefficients were estimated for four different scenarios of wall coupling: thermal continuity, adiabatic boundary conditions, gap of 100 μm, and gap of 1 mm. As expected from previous evidences, the thermal discontinuity between the solid foam matrix and the wall dramatically affects the overall heat transfer performance of the foam bed system, when conduction in the solid phase is the dominant mechanism. However, the difference between the performance of the coupled and uncoupled configuration decreases when increasing the flow rate and the thermal properties of the fluid phase. This can lead to the opposite case where convection in the fluid phase is the dominant contribution to the heat transfer, such as in the simulation with water at the highest flow rates.

For the cases of thermal discontinuity between the wall and the support, new correlations for the wall heat transfer coefficient were derived and are proposed in this paper in the form of a static and a dynamic term depending on the Peclet number. The range of validity in terms of Peclet number covers four orders of magnitude (between 2 and 6E+4) for the case of a 100 μm gap (Eq. (16)), and two orders of magnitude (between 2 and 749) for the case of a 1 mm gap (Eq. (18)). The effect of the gap size on the wall heat transfer coefficient was found to be significant only for the static contribution of the above-mentioned correlations.

In conclusion, the new correlations derived in this work enable to predict the wall heat transfer coefficient of metal open-cell foam reactors for a wide range of flow rates and working fluids. Moreover, it is possible to evaluate whether the wall heat transfer or the effective radial conductivity is the controlling parameter for the radial heat transfer. The generally expected and assumed promising heat transfer performance of metal open-cell foams used in catalytic reactors can be confirmed with the results of this work. However, as an additional important new aspect the strong dependence of the heat transfer on the Peclet number with turbulent flow and on the estimated tolerance with the wall has been revealed and analyzed in detail. The results underline the crucial importance of the proper placement and fitting of the foam inside the reactor in order to exploit the full potential of these promising new catalyst support structures.

Acknowledgments

The authors gratefully acknowledge the funding of the German Research Foundation (DFG), which, within the framework of its "Excellence Initiative" supports the Cluster of Excellence "Engineering of Advanced Materials" at the University of Erlangen-Nürnberg (www.eam.uni-erlangen.de).

Furthermore, we thank the Helmholtz Association for funding within the frame of the Helmholtz Energy Alliance "Energy Efficient Multiphase Chemical Processes".

The authors from Politecnico di Milano acknowledge funding by the Italian Ministry of Education, University and Research, Rome (MIUR, Progetti di Ricerca Scientifica di Rilevante Interesse Nazionale, prot. 2010XFT2BB) within the project IFOAMS ("Intensification of Catalytic Processes for Clean Energy, Low-Emission Transport and Sustainable Chemistry using Open-Cell Foams as Novel Advanced Structured Materials").

References

[1] D. Edouard, M. Lacroix, C.P. Huu, F. Luck, Pressure drop modeling on SOLID foam: state-of-the art correlation, Chem. Eng. J. 144 (2) (2008) 299–311.
[2] A. Inayat, J. Schwerdtfeger, H. Freund, C. Körner, R.F. Singer, W. Schwieger, Periodic open-cell foams: pressure drop measurements and modeling of an ideal tetrakaidecahedra packing, Chem. Eng. Sci. 66 (2011) 2758–2763.
[3] M. Klumpp, A. Inayat, J. Schwerdtfeger, C. Körner, R.F. Singer, H. Freund, W. Schwieger, Periodic open cellular structures with ideal cubic cell geometry: effect of porosity and cell orientation on pressure drop behaviour, Chem. Eng. J. 242 (2014) 364–378.
[4] A. Inayat, H. Freund, A. Schwab, T. Zeiser, W. Schwieger, Predicting the specific surface area and pressure drop of reticulated ceramic foams used as catalyst support, Adv. Eng. Mater. 13 (2011) 990–995.
[5] A. Inayat, H. Freund, T. Zeiser, W. Schwieger, Determining the specific surface area of ceramic foams: the tetrakaidecahedra model revisited, Chem. Eng. Sci. 66 (2011) 1179–1188.
[6] B. Dietrich, G. Schell, E.C. Bucharsky, R. Oberacker, M.J. Hoffmann, W. Schabel, M. Kind, H. Martin, Determination of the thermal properties of ceramic sponges, Int. J. Heat Mass Transfer 53 (1) (2010) 198–205.
[7] C. Cristiani, C.G. Visconti, S. Latorrata, E. Bianchi, E. Tronconi, G. Groppi, P. Pollesel, Coating method for Ni/MgAl2O4 deposition on metallic foam, Stud. Surf. Sci. Catal. 175 (2010) 653–656.
[8] C. Cristiani, E. Finocchio, S. Latorrata, C.G. Visconti, E. Bianchi, E. Tronconi, G. Groppi, P. Pollesel, Activation of metallic open-cell foams via washcoat deposition of $Ni/MgAl_2O_4$ catalysts for steam reforming reaction, Catal. Today 197 (2012) 256–264.
[9] A.G. Dixon, Correlations for wall and particle shape effects on fixed bed bulk voidage, Can. J. Chem. Eng. 66 (1988) 705–708.
[10] E. Bianchi, T. Heidig, C.G. Visconti, G. Groppi, H. Freund, E. Tronconi, An appraisal of the heat transfer properties of metallic open-cell foams for strongly exo-/endothermic catalytic processes in tubular reactors, Chem. Eng. J. 198–199 (2012) 512–528.
[11] G.F. Froment, Design of fixed bed catalytic reactors based on effective transport models, Chem. Eng. Sci. 17 (1962) 849–859.
[12] J.T. Richardson, D. Remue, J.-K. Hung, Properties of ceramic foam catalyst supports: mass and heat transfer, Appl. Catal. A Gen. 250 (2) (2003) 319–329.
[13] V.V. Calmidi, R.L. Mahajan, Effective thermal conductivity of high porosity fibrous metal foams, J. Heat Transfer 121 (2) (1999) 466–471.
[14] D.P. Haack, K.R. Butcher, T. Kim, T.J. Lu, Novel Lightweight Metal Foam Heat Exchangers, American Society of Mechanical Engineers, New York, NY, United States, 2001.
[15] T.J. Lu, H.A. Stone, M.F. Ashby, Heat transfer in open-cell metal foams, Acta Mater. 46 (10) (1998) 3619–3635.
[16] W. Lu, C.Y. Zhao, S.A. Tassou, Thermal analysis on metal-foam filled heat exchangers. Part I: metal-foam filled pipes, Int. J. Heat Mass Transfer 49 (15) (2006) 2751–2761.
[17] Y. Peng, J.T. Richardson, Properties of ceramic foam catalyst supports: one-dimensional and two-dimensional heat transfer correlations, Appl. Catal. A Gen. 266 (2004) 235–244.
[18] B. Dietrich, M. Kind, H. Martin, Axial two-phase thermal conductivity of ceramic sponges – experimental results and correlation, Int. J. Heat Mass Transf. 54 (2011) 2276–2282.
[19] D. Edouard, T.T. Huu, C.P. Huu, F. Luck, D. Schweich, The effective thermal properties of solid foam beds: experimental and estimated temperature profiles, Int. J. Heat Mass Transfer 53 (19–20) (2010) 3807–3816.
[20] K. Pangarkar, T.J. Schildhauer, J.R. van Ommen, J. Nijenhuis, J.A. Moulijn, F. Kapteijn, Heat transport in structured packings with co-current downflow of gas and liquid, Chem. Eng. Sci. 65 (2010) 420–426.
[21] E. Bianchi, T. Heidig, C.G. Visconti, G. Groppi, H. Freund, E. Tronconi, Heat transfer properties of metal foam supports for structured catalysts: wall heat transfer coefficient, Catal. Today 216 (1) (2013) 121–134.
[22] A.G. Dixon, M. Nijemeisland, CFD as a design tool for fixed-bed reactors, Ind. Eng. Chem. Res. 40 (2001) 5246–5254.
[23] M. Nijemeisland, A.G. Dixon, CFD study of fluid flow and wall heat transfer in a fixed bed of spheres, AIChE J. 50 (2004) 906–921.
[24] C. von Scala, M. Wehrli, G. Gaiser, Heat transfer measurements and simulation of KATAPAK-M® catalyst supports, Chem. Eng. Sci. 54 (1999) 1375–1381.
[25] P.W.A.M. Wenmakers, J. van der Schaaf, B.F.M. Kuster, J.C. Schouten, Enhanced liquid–solid mass transfer by carbon nanofibers on solid foam as catalyst support, Chem. Eng. Sci. 65 (2010) 247–254.
[26] C. Hutter, A. Zenklusen, S. Kuhn, P.R. von Rohr, Large eddy simulations of flow through a streamwise-periodic structure, Chem. Eng. Sci. 66 (2011) 519–529.
[27] OpenFOAM project web pages, <http://www.openfoam.com>, 2013.
[28] H.G. Weller, G. Tabor, H. Jasak, C. Fureby, A tensorial approach to computational continuum mechanics using object orientated techniques, Comp. Phys. 12 (6) (1998) 620–631.
[29] H. Jasak, A. Jemcov, Z. Tukovic, OpenFOAM: A C++ Library for Complex Physics Simulations, International Workshop on Coupled Methods in Numerical Dynamics IUC, Dubrovnik, Croatia, September 2007.
[30] J. Große, B. Dietrich, H. Martin, M. Kind, J. Vicente, E.H. Hardy, Volume image analysis of ceramic sponges, Chem. Eng. Technol. 31 (2) (2008) 307–314.
[31] M.H. Pedras, M.J. de Lemos, Macroscopic turbulence modeling for incompressible flow through undeformable porous media, Int. J. Heat Mass Transfer 44 (6) (2001) 1081–1093.
[32] F.R. Menter, M. Kuntz, R. Langtry, Ten years of industrial experience with the SST turbulence model, turbulence, Heat Mass Transfer 4 (2003) 625–632.
[33] W. Sutherland LII, The viscosity of gases and molecular force, London, Edinburgh, Dublin Philos. Mag. J. Sci. 36 (223) (1893) 507–531.

[34] A. Kopanidis, A. Theodorakakos, E. Gavaises, D. Bouris, 3D numerical simulation of flow and conjugate heat transfer through a pore scale model of high porosity open cell metal foam, Int. J. Heat Mass Transfer 53 (11) (2010) 2539–2550.
[35] S.V. Patankar, C.H. Liu, E.M. Sparrow, Fully developed flow and heat transfer in ducts having streamwise-periodic variations of cross-sectional area, J. Heat Transfer 99 (1977) 180–186.
[36] B. Dietrich, Pressure drop correlation for ceramic and metal sponges, Chem. Eng. Sci. 74 (2012) 192–199.
[37] G.I. Garrido, F.C. Patcas, S. Lang, B. Kraushaar-Czarnetzki, Mass transfer and pressure drop in ceramic foams: a description for different pore sizes and porosities, Chem. Eng. Sci. 63 (21) (2008) 5202–5217.
[38] A.A. Zukauskas, Convective heat transfer in cross-flow, in: S. Kakac, R.K. Shah, W. Aung (Eds.), Handbook of Single-Phase Convective Heat Transfer, Wiley, New York, 1987.
[39] G. Groppi, L. Giani, E. Tronconi, Generalized correlation for gas/solid mass-transfer coefficients in metallic and ceramic foams, Ind. Eng. Chem. Res. 46 (12) (2007) 3955–3958.
[40] B. Dietrich, Heat transfer coefficients for solid ceramic sponges – experimental results and correlation, Int. J. Heat Mass Transfer 61 (2013) 627–637.
[41] D. Vervloet, M.R. Kamali, J.J.J. Gillissen, J. Nijenhuis, H.E.A. van den Akker, F. Kapteijn, J.R. van Ommen, Intensification of co-current gas–liquid reactors using structured catalytic packings: a multiscale approach, Catal. Today 147S (2009) S138–S143.
[42] A.G. Dixon, Thermal resistance models of packed-bed effective heat transfer parameters, AIChE J. 31 (5) (1985) 826–834.
[43] C.-H. Li, B.A. Finlayson, Heat transfer in packed beds—a reevaluation, Chem. Eng. Sci. 32 (9) (1977) 1055–1066.
[44] Z. Dai, K. Nawaz, Y. Park, Q. Chen, A.M. Jacobi, A comparison of metal-foam heat exchangers to compact multilouver designs for air-side heat transfer applications, Heat Transfer Eng. 33 (1) (2012) 21–30.
[45] I. Ghosh, Heat-transfer analysis of high porosity open-cell metal foam, J. Heat Transfer 130 (3) (2008) 6.
[46] S. Mancin, C. Zilio, L. Rossetto, A. Cavallini, Foam height effects on heat transfer performance of 20 ppi aluminum foams, Appl. Therm. Eng. 49 (2012) 55–60.
[47] F.P. Incropera, A.S. Lavine, D.P. DeWitt, Fundamentals of Heat and Mass Transfer, John Wiley & Sons Incorporated, 2011.
[48] R. Lemlich, A theory for the limiting conductivity of polyhedral foam at low density, J. Colloid Interface Sci. 64 (1) (1978) 107–110.
[49] D.-Y. Lee, K. Vafai, Analytical characterization and conceptual assessment of solid and fluid temperature differentials in porous media, Int. J. Heat Mass Transfer 42 (3) (1999) 423–435.
[50] N. Wakao, S. Kaguei, Heat and Mass Transfer in Packed Beds, Gordon and Breach, New York, 1982.
[51] J. Beek, E. Singer, A procedure for scaling-up a catalytic reactor, Chem. Eng. Prog. 47 (10) (1951) 534.
[52] J. Villadsen, M.L. Michelsen, Solution of Differential Equation Models by Polynomial Approximation, vol. 7, Prentice-Hall, Englewood Cliffs NJ, 1978.
[53] A. Bhattacharya, W. Calmidi, R.L. Mahajan, Thermophysical properties of high porosity metal foams, Int. J. Heat Mass Transfer 45 (2002) 1017–1031.
[54] V. Specchia, G. Baldi, S. Sicardi, Heat transfer in packed bed reactors with one phase flow, Chem. Eng. Commun. 4 (2–3) (1980) 361–380.
[55] M. Dente, A. Collina, Verifica di un Reattore Tubolare per l'Ossidazione del Metanolo a Formaldeide, La Chimica e l'Industria 48 (6) (1966) 581–588.
[56] P.J. Roache, Quantification of uncertainty in computational fluid dynamics, Annu. Rev. Fluid Mech. 29 (1997) 123–160.